

4-1-2023

Computational Analysis of Water Dynamics in AOT Reverse Micelles

Max Crowder

Frozan Tahiry

Isabel Lizarraga

Stephanie Rodriguez

Nathaly Peña

See next page for additional authors

Follow this and additional works at: https://digitalcommons.csumb.edu/biochem_fac

This Article is brought to you for free and open access by the Department of Biology and Chemistry at Digital Commons @ CSUMB. It has been accepted for inclusion in Biology and Chemistry Faculty Publications and Presentations by an authorized administrator of Digital Commons @ CSUMB. For more information, please contact digitalcommons@csumb.edu.

Authors

Max Crowder, Frozan Tahiry, Isabel Lizarraga, Stephanie Rodriguez, Nathaly Peña, and Arun K. Sharma



Computational analysis of water dynamics in AOT reverse micelles

Max Crowder, Frozan Tahiry, Isabel Lizarraga, Stephanie Rodriguez, Nathaly Peña, Arun K. Sharma*

Department of Biology and Chemistry, California State University, Monterey Bay, Seaside, CA 93955, United States



ARTICLE INFO

Article history:

Received 14 November 2022

Revised 18 January 2023

Accepted 26 January 2023

Available online 30 January 2023

Keywords:

Reverse micelles

Water dynamics

Molecular dynamics simulation

Rotational anisotropy

Interfacial water

ABSTRACT

Aerosols can be modeled for detailed investigations using reverse micelles in the laboratory as well as in computational simulations. A long-standing question in the description of confined water under these conditions is that of a two-state model of core – interface or a three-state model of core – intermediate – interface. In this work, we present results of analysis of water dynamics inside reverse micelles from fully atomistic molecular dynamics simulations. The size and composition of reverse micelles is expressed through w_0 , the ratio of the number of water molecules to the number of surfactant molecules. Reverse micelles of diverse sizes, with w_0 ranging from 5 to 20, were constructed with Sodium bis(2-ethylhexyl) sulfosuccinate (AOT) surfactant and simulated within isoctane solvent. Residence time and diffusion coefficients, in the simulations, both behaved increasingly like bulk water with the increase in size of reverse micelles. Rotational anisotropy autocorrelation was modeled using exponential functions in the short time range of 10–20 ps and longer time data were modeled as a power law fit. Similarly, the diffusion of water in the reverse micelles was also modeled on a power law fit. All these metrics demonstrate a clear progression towards bulk water behavior as the reverse micelle size increases. Additionally, our results also support a 3-layer model of water in a reverse micelle of core – intermediate – interface. These results extend the understanding of water dynamics in reverse micelles and provide further evidence for the 3-layer model.

© 2023 The Author(s). Published by Elsevier B.V.

1. Introduction

Water, despite its importance in most systems, is still not fully understood due to its anomalous properties and differing behavior under constrained, interfacial, and bulk conditions. [1–4] Under these constrained and interfacial conditions, water is biologically and materially functional [2,4]. The extensive research carried out in the past few decades has established that confined water has very different physicochemical properties compared to bulk water [5–7]. Some properties that are the hallmark of confined water are reduced polarity, perturbed hydrogen bonded network, and structural reordering at the interfacial region [8].

Reverse micelles (RMs) have served various functions, from bioreactors to solubility vehicles [9,10] and are relatively well studied with experimental methods [11–15]. Sodium bis(2-ethylhexyl) sulfosuccinate (AOT) is a common surfactant used in studying reverse micelles in both experimental and computational settings, having an anionic head and a large, branched nonpolar tail structure allowing for dissolution of large amounts of water in organic solution. [1,16–18] AOT's two-tail structure enables

reverse micelle formation without the addition of a cosurfactant, making AOT useful for a wide range of investigations and applications [19].

The fact that polar regions of RMs can be manipulated, expand their application even further in various fields. The effect of various ionic liquid substitutes on the nanoaggregates of RMs have also been studied; and the results suggest a shape transition of core droplets from spherical in $[\text{Na}][\text{AOT}]$ to cylindrical in the 1-butyl-3-methylimidazolium, $[\text{BMIM}]^+ [\text{AOT}]^-$ solution [20]. This is evidence that RMs are composed of monomeric amphiphilic building blocks; and therefore, any manipulation at the monomer level seems to offer an easy control over the structural aspect of large self-aggregated systems. As a result, giving RMs, potential applications in synthetic chemistry, separation technology, and many other domains [21].

RMs have also been extensively utilized as a model system for water and other biomolecules in crowded and constrained environments [1,3,22]. Water within reverse micelles does not behave uniformly; water closer to the surfactant, the interfacial layer, displays dynamics significantly different from an unconfined bulk environment. Investigations on dynamic behavior of water as a function of distance from the interfacial layer have revealed slower dynamical behaviour [23] of confined water relative to bulk

* Corresponding author.

E-mail address: arsharma@csumb.edu (A.K. Sharma).

environment. Nanoconfinement of water in RMs also affects proton transfer and results in a mechanism called proton hopping [5]. Additionally, a marked slowdown in transfer rates of protons has been discovered in nanoconfined systems such as RMs [24].

To better replicate the behavior of reverse micelles various model systems have been developed to represent their behavior for theoretical and computational analyses. Earlier experimental studies on reverse micelles established a bi-layer model for reverse micelles consisting of an inner core and an outer interfacial layer. This model has been used rather extensively in many studies as a basis for reverse micelle modeling, to differentiate the dynamics of core 'bulk-like' water and interfacial confined water which both exist within the RM [8,23,25]. However, more recent studies have suggested that the core-interface bi-layer model is an oversimplification of reverse micelle behavior, and a multilayered model would be a superior representation of reverse micelle behavior. [8,23,25].

The core-shell or core-interface model has limitations, since the dynamics of the "shell" water depends on the size of the micelle [23]. The core-interface bi-layer model is well suited to larger reverse micelles; however, it starts to break down for smaller RMs with w_0 less than 10 [26]. This has been posited to happen due to the collective nature of water dynamics for smaller reverse micelles. Measurements of vibrational echo peak shifts have provided information about molecular rotation and confirm that the core-shell separation is appropriate for static observables but not for dynamic observables [27–29]. In this investigation, we utilized fully atomistic molecular dynamics (MD) simulations of various sized aqueous AOT reverse micelles to analyze the dynamics of water and to provide further evidence to support a three-layer water model. MD simulations of reverse micelles have played a pivotal role in shedding light on structural and dynamic properties, surfactant counter-ion mobilities, and ion pairings in such assemblies [30–41]. Our results are based on an analysis of dynamic and static properties of water and the entire reverse micelle assembly for a variety of reverse micelle compositions. Previous results in this domain have used different compositions of reverse micelles to arrive at the three-layer model [16,42]. Our reverse micelle compositions follow those of Abel et al. [38] with the TIP3P [43] water model and provide further supporting evidence for the three-layer model.

2. Methods

All-atom MD simulations for the L2 phase of the ternary system composed of AOT and H₂O in isoctane (ISO) were conducted. All simulations were run using GROMACS [44–49] software package with temperature and pressure at 298 K and 1 bar respectively. Simulation trajectories ranged from 100 ns to 150 ns to collect detailed dynamical information. All simulations were performed utilizing fully atomistic CHARMM27 [50–53] force fields in the NPT ensemble. Simulations started with a spherical reverse micelle immersed in ISO. The entire assembly was constructed using Packmol. [54] During NVT equilibration stage, the reverse micelle was restrained, and the solvent ISO allowed to move freely. After NVT equilibration the restraints holding the reverse micelle were released slowly for a completely unrestrained run. The starting configurations were minimized to 100 kJ/mol/nm. All simulations were carried out in a cubic box of at least 6.5 nm side length. CHARMM27 [51] parameters implemented for AOT and ISO and utilized in previous molecular dynamics studies were applied [38]. The TIP3P [43] model was used to describe water molecules. The particle mesh Ewald method [55] implemented in GROMACS was used to calculate the long-range electrostatics in the system. The production MD stage was run for a duration of 100 – 150 ns

with a timestep of 2 fs. Each simulation was executed from two distinct starting configurations. The calculated properties are in excellent agreement between those two independent simulation trajectories. Simulations and data analysis were carried out on the EXPANSE [56] supercomputer at the San Diego Supercomputing Center through an XSEDE [57] allocation. The simulation labeled "bulk" is a simulation of water molecules in a cubic box of side 6 nm and under similar temperature and pressure conditions as the reverse micelle simulations. All analysis was carried out using the tools provided with the GROMACS simulation package. Mathematica was used to create all the plots, data fitting, and for any numerical processing of the data derived from the MD simulations. The composition for each simulation is specified in Table 1.

3. Results & discussion

3.1. Rotational relaxation analysis

The rotational anisotropy autocorrelation function was calculated from our simulations by taking the dot product of the unit vectors \hat{u} in the direction of the O–H bonds and calculating the correlation function of the second Legendre polynomial [16].

$$C_2(t) = P_2 < \hat{u}(t) \cdot \hat{u}(0) >$$

$$\text{where } P_2(x) = \frac{3x^2-1}{2} \text{ and } x = \text{Cos}(\theta) = \hat{u}(t) \cdot \hat{u}(0)$$

Rotational anisotropy data was fitted to three different models, finding agreement with prior studies that a tri-exponential, stretched exponential, and power law fit were valid with R^2 values greater than 0.99. The excellent agreement of our data with these functional forms provides a strong validation for these models and consistency with previous work in this domain [58].

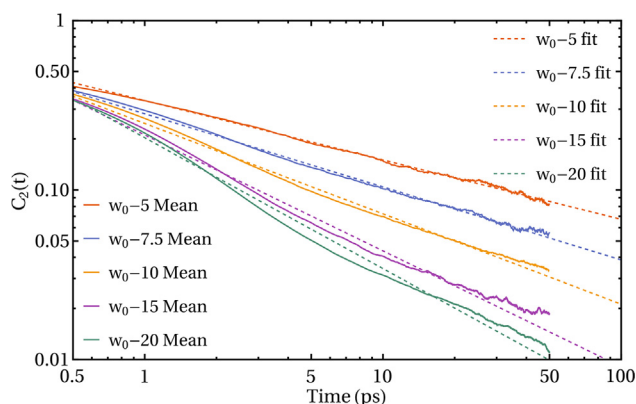
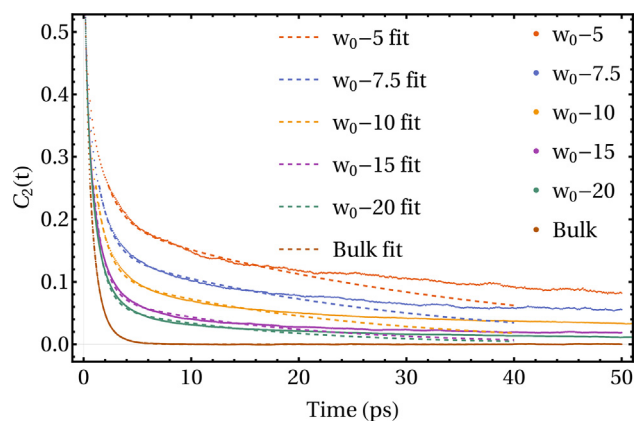
The power law fit was implemented through a nonlinear scalar model, $\alpha * t^{-\beta}$, to model the behavior of water's rotational anisotropy decay for long time scales as shown in Fig. 1. This model is a modification of the linear scalar power law used by other authors and is in excellent qualitative agreement [58]. The power law modifiers, α and β display a limiting trend towards their bulk values.

The triexponential fit, shown in Fig. 2, is valid for the first 20 ps of the simulation before it deviates from the data and is described by $C_0 e^{-\frac{x}{\tau_0}} + C_1 e^{-\frac{x}{\tau_1}} + C_2 e^{-\frac{x}{\tau_2}}$. Each term in the tri-exponential fit corresponds to a layer of the water in the RM. Thus, this model assumes three layers, the interface, intermediate, and core, from outwards towards the interior, respectively. The interfacial layer has the slowest rotational decay, and the intermediate layer displays the fastest rotational decay [16,26]. The tri-exponential fit is only viable for ~ 20 ps, after which another fit must be used. This necessitates power law fits for long time behavior. As seen in Fig. 2, the initial decay is much faster for larger reverse micelles, $w_0 \geq 10$. The behavior of the water as the size of the reverse micelle increases is increasingly like that of bulk [23]. A simplification of the triexponential fit can also be used; a stretched exponential fit of the form $e^{-\left(\frac{x}{\tau}\right)^\beta}$. Both, β and τ , are proportional to w_0 , and both display a limiting approach to the respective variables for bulk water simulations. The stretched exponential fit, shown in Fig. S1 (Supporting Information), however, is only valid for ~ 10 ps, and to model longer time frame, the power-law fit shown in Fig. 1 is necessary.

A noticeable trend appears in the data, that as the w_0 increases, the behavior of the water also trends toward bulk or unconstrained water as shown in Fig. 2. For all three autocorrelation models, as w_0 increases the models increasingly resemble the models for bulk water. Experimental work has shown that there is longer rotational anisotropy decay in larger reverse micelles as compared with smaller systems, indicating that as time passes the directional depen-

Table 1Simulation compositions for each reverse micelle, represented by w_0 , showing the number of molecules present. A sodium counterion is present for each AOT molecule.

$w_0 = [\text{H}_2\text{O}]/[\text{AOT}]$	H ₂ O	AOT	Isooctane	Total molecules
5	210	42	1,500	1,794
7.5	465	62	2,536	3,125
10	980	98	3,500	4,676
15	2,835	189	6,000	9,213
20	6,040	302	23,474	30,118
Bulk water	7,085	0	0	7,085

**Fig. 1.** Rotational anisotropy decay on a log-log plot showing the increased rate of decay as system size increases, reflecting increased behavior of ‘bulk like’ water in larger systems.**Fig. 2.** The rotational anisotropy decay shows excellent agreement with fit to a tri-exponential function up to the first 20 ps.

dence of H₂O molecule rotation decreases at greater rates in larger systems with less constraint, i.e. bulk water or large reverse micelles, than in systems with more confinement, i.e. smaller reverse micelles. [16,27] These results agree with our modeling of rotational anisotropy decay. However, investigations into impact of nanoconfinement in AOT reverse micelles of binding interactions between phenosafranin and safranin-O with DNA duplex arrive at the conclusion that even with large reverse micelles (w_0 -greater than 10), bulk-like behavior is not truly achieved. [59,60].

3.2. Diffusion analysis

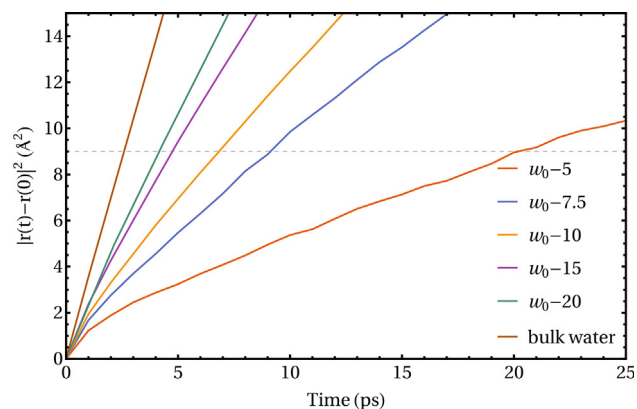
The mean squared displacement (MSD) of water from initial position was calculated to determine the diffusion constant via the Einstein relation. The residence time (τ_w) was determined as the time needed for the MSD to traverse a distance equivalent to the square of the molecule’s diameter. The residence time is noted

when $\text{MSD} = 9 \text{ \AA}^2$ in the simulations. A power law of the form, t^α , was fit for the MSD for all simulations and is shown in the [supporting information](#). This is consistent with prior work [38] displaying that the smaller reverse micelles having slower rates of diffusion. The parameter α in the model also trends toward the α in the fitted bulk model in a limiting manner.

The residence time can be a good indicator of diffusion intensity. The water of larger w_0 s behaves more like bulk water than that of smaller w_0 s (Fig. 3); and the τ_w is seen to decrease as the w_0 increases, indicating that the water in the reverse micelle behaves increasingly like that of bulk as it increases in size. This may be a result of the curvature of the reverse micelle acting as a constraint. The increased diffusion speeds are reflected in lower residence times.

3.3. Hydrogen bonding

Typically, a hydrogen bond is defined to exist when water molecules are within 3.5 Å and the Hydrogen-Donor-Acceptor angle is less than or equal to 30° [61]. The number of hydrogen bonds formed by each water molecule was calculated using gmh_bonds provided with the GROMACS package. It determines hydrogen bonds that satisfy distance and angle constraint, as well as hydrogen bonds that only satisfy the distance constraint. Here, the expectation is that the confinement of water in the reverse micelles will reduce more water-water interactions that would have been labeled as hydrogen bonds due to reduced orientational freedom for water molecules. The distribution plot is shown in Fig. 4. The distribution tightens, indicating a greater population of water is under less constraint as the reverse micelle increases in size, this trend follows in limiting fashion towards bulk. This is most likely due to the reduced orientational freedom for water molecules near the surfactant interface. Additionally, the average number of hydrogen bonds per molecule increases and trend

**Fig. 3.** Mean square displacement against time. The dashed horizontal line at 9 \AA^2 is the square of the diameter of the water molecule. The residence time, τ_w can be seen to decrease with increasing amounts of water in the RM and approaches that of bulk water.

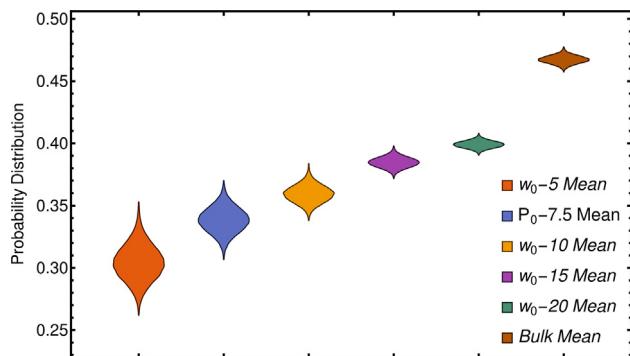


Fig. 4. Distribution plot of the number of hydrogen bonds that satisfy angle and distance constraint divided by the number of hydrogen bonds that only satisfy the distance constraint.

toward bulk in limiting fashion as the reverse micelle increases in size as shown in Fig. 5.

3.4. Dipole moment

The dipole autocorrelation function was calculated over the total dipole moment of the simulation space via a second order Legendre polynomial. Dipole autocorrelation was averaged over all water molecules for the full trajectory of the simulation. The dipole correlation of the water molecules within the reverse micelle was computed and the data fit to multiple exponential fits: a tri-exponential fit, stretched exponential fit, and a power law fit, in agreement with prior studies [28,62]. The data fits very well to a triexponential model, shown in Fig. 6, suggesting three layers with each having differing behaviors. As core volume increases with increasing w_0 , overall, the RM increasingly behaves like bulk, like the tri-exponential model for rotational anisotropy decay. This trend was also visible when dipole autocorrelation was modeled by a stretched exponential, and power law fit. The power law fits the data well as shown in Fig. 7. The forms for these fits are identical to the stretched exponential and power law fits that were used to model rotational anisotropy, suggesting that dipole correlation & rotational anisotropy decay are affected in the same manner.

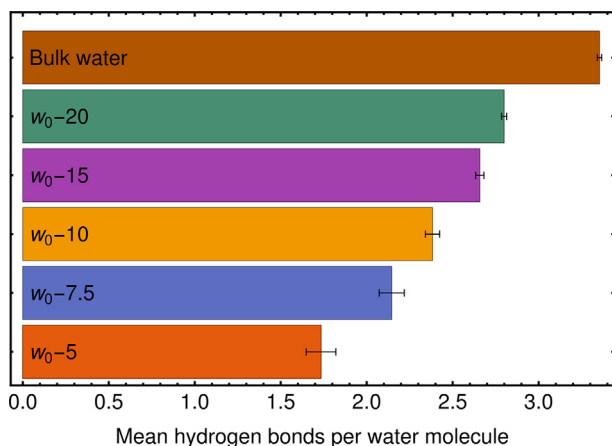


Fig. 5. Mean number of hydrogen bonds per water molecule for each simulation. The reported number is derived from the average of two independent trajectories for each simulation.

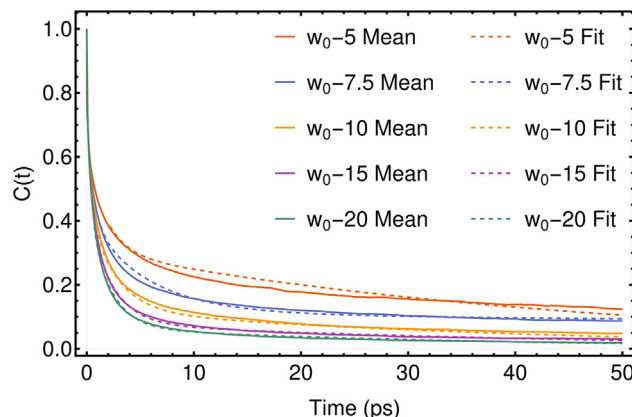


Fig. 6. Dipole autocorrelation function fits well to a tri-exponential function up to the first 50 ps., $C_0 e^{-\frac{t}{\tau_0}} + C_1 e^{-\frac{t}{\tau_1}} + C_2 e^{-\frac{t}{\tau_2}}$

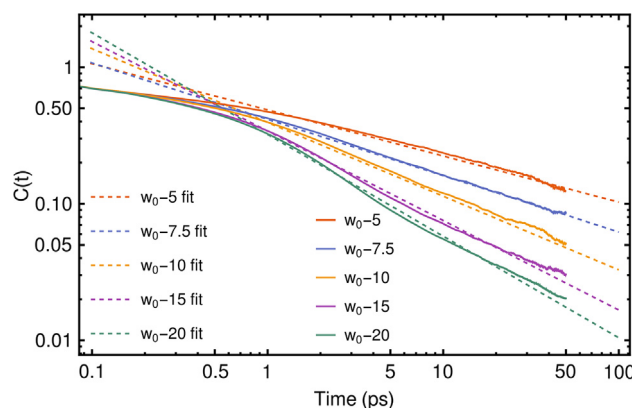


Fig. 7. Power laws model the longer-term dipole moment autocorrelation after 1 ps.

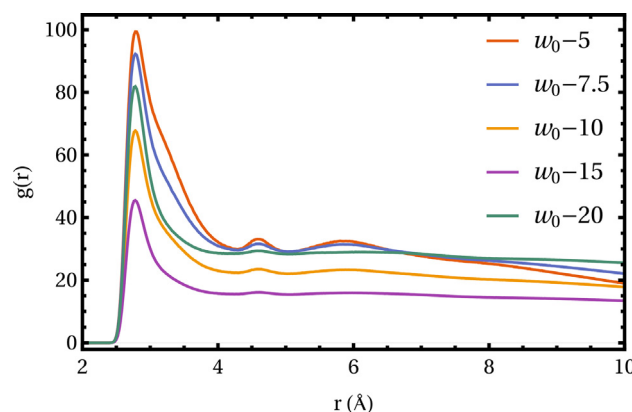


Fig. 8. Radial distribution function plots for $g(O-O)$ for water molecules in the reverse micelle simulations.

3.5. Radial distribution functions

The radial distribution function (RDF) describing the distribution of water from the center of mass of the reverse micelle was calculated for all simulations. The water population was found at different distances from the center of the reverse micelle by determining the area under the curve of the RDF, using the relative minima of the RDF as limits representing a divide in each layer of water population from the reverse micelle.

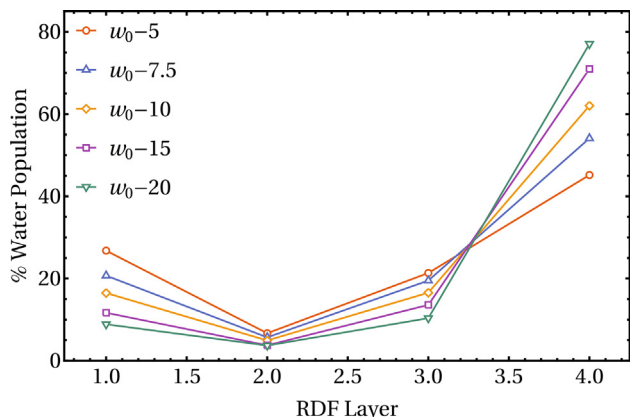


Fig. 9. Normalized water population per layer from the radial distribution function for the oxygen–oxygen distribution function.

The radial distribution functions of the water population within the RM allows for the water in the reverse micelle to be separated into layers wherein the minimum of the RDF serves as a boundary between layers and the percent of the overall water molecule population residing in that layer could be calculated. The oxygen–oxygen, $g(O-O)$ is shown in Fig. 8 for the reverse micelle simulations. There is a clear demarcation of three layers of arrangement corresponding to 3 distinct peaks in the $g(r)$ plots. The amount of water in each of these layers was calculated to provide an estimate of the distribution of water in these layers. The resulting distribution is shown in Fig. 8. The population of water in the core layer, which is the last layer in Fig. 9, increases as w_0 increases and provides an internal consistency check for the simulations. We employed the minima of the function to categorize water and demonstrate that the water population of these categories each have a distinct trend. Additionally, these RDF categories, “layers”, correlate with the multilayer RM model. The RDF layer 4 increased in population suggesting in our model that there is more bulk-like water in larger systems. While RDF layer 1 displays an inverse relationship to layer 4, which matches our assumptions about interfacial water amounts. Thus, RDF analysis can be utilized to quantify amounts of water that tend to behave in a certain way.

3.6. Shape

The reverse micelles were unrestrained during the simulation and sample varied morphologies. All simulation trajectories display a rapid deformation from their initial spherical shape, which is consistent with previous works [20,38]. The shape of the reverse micelle can be approximated as an ellipsoid and thus three semi-axes, a , b , c , and three moments of inertia I_1 , I_2 , I_3 where $I_1 > I_2 > I_3$ can be determined, as well as the eccentricity of the approximated ellipsoid, e [38,40].

$$I_1 = \frac{1}{5}M(a^2 + b^2)$$

$$I_2 = \frac{1}{5}M(a^2 + c^2)$$

$$I_3 = \frac{1}{5}M(b^2 + c^2)$$

$$e = \sqrt{1 - \frac{c^2}{a^2}}$$

Table 2 reports the parameters for ellipsoid semi-axes, eccentricity, and moments of inertia for each reverse micelle simulation

Table 2
Semi-axes of micellar ellipsoid, radius of gyration, and eccentricity. Radii of gyration determined from semi-axes $a > b > c$ computed from the three moments of inertia (I_1, I_2, I_3).

w_0	$a(\text{\AA})$	$b(\text{\AA})$	$c(\text{\AA})$	$\langle s_i \rangle$	e	I_1 (10^6 amu \AA^2)	I_2 (10^6 amu \AA^2)	I_3 (10^6 amu \AA^2)	$\langle R_g \rangle$ (\AA)	$R_{\text{AOT}}(\text{\AA})$
5	26.842 ±0.0050	17.7466 ±0.0033	15.3024 ±0.0017	1.7591 ±0.0005	0.81387 ±0.0001	4.6782 ±0.0011	4.3121 ±0.0012	2.4886 ±0.0005	15.9638 ±0.0013	19.3370 ±0.0005
7.5	28.437 ±0.0060	21.459 ±0.0040	17.0297 ±0.0033	1.6876 ±0.0006	0.79855 ±0.0001	10.3558 ±0.0022	8.9828 ±0.0024	5.9015 ±0.0016	17.7375 ±0.0011	21.7966 ±0.0007
10	38.742 ±0.0140	27.5198 ±0.0070	21.487 ±0.0060	1.8154 ±0.0010	0.82367 ±0.0002	27.776 ±0.010	24.150 ±0.011	14.747 ±0.005	23.3609 ±0.0029	28.3387 ±0.0014
15	50.765 ±0.0140	38.689 ±0.0100	29.008 ±0.0090	1.7556 ±0.0009	0.81221 ±0.0001	110.854 ±0.032	92.897 ±0.034	64.658 ±0.023	31.4519 ±0.0027	38.3615 ±0.0022
20	70.134 ± 0.028	42.529 ± 0.016	33.751 ± 0.009	2.1167 ± 0.010	0.87242 ± 0.0002	334.25 ± 0.15	296.86 ± 0.20	70.134 ± 0.028	145.58 ± 0.008	46.466 ± 0.004

- [25] H.-S.-S. Tan, I.R. Piletic, M.D. Fayer, Orientational dynamics of water confined on a nanometer length scale in reverse micelles, *J. Chem. Phys.* 122 (2005), <https://doi.org/10.1063/1.1883605>.
- [26] A. Baksi, P.K. Ghorai, R. Biswas, Dynamic Susceptibility and Structural Heterogeneity of Large Reverse Micellar Water: An Examination of the Core-Shell Model via Probing the Layer-wise Features, *J. Phys. Chem. B* 124 (2020) 2848–2863, <https://doi.org/10.1021/acs.jpcc.9b11895>.
- [27] I.R. Piletic, H.-S. Tan, M.D. Fayer, Dynamics of Nanoscopic Water, *J. Phys. Chem. B* 109 (2005) 21273–21284.
- [28] I.R. Piletic, D.E. Moilanen, D.B. Spry, N.E. Levinger, M.D. Fayer, Testing the Core/Shell Model of Nanoconfined Water in Reverse Micelles Using Linear and Nonlinear IR Spectroscopy, *Chem. A Eur. J.* 110 (2006) 4985–4999, <https://doi.org/10.1021/jp061065c>.
- [29] H.S. Tan, I.R. Piletic, R.E. Riter, N.E. Levinger, M.D. Fayer, Dynamics of water confined on a nanometer length scale in reverse micelles: Ultrafast infrared vibrational echo spectroscopy, *Phys. Rev. Lett.* 94 (2005) 1–4, <https://doi.org/10.1103/PhysRevLett.94.057405>.
- [30] J. Faeder, B.M. Ladanyi, Molecular Dynamics Simulations of the Interior of Aqueous Reverse Micelles, *J. Phys. Chem. B* 104 (2000) 1033–1046, <https://doi.org/10.1021/jp993076u>.
- [31] A. v. Nevidimov, V.F. Razumov, Molecular dynamics simulations of AOT reverse micelles' self-assembly, *Mol Phys.* 107 (2009) 2169–2180. 10.1080/00268970903203736.
- [32] D.J. Tobias, M.L. Klein, Molecular Dynamics Simulations of a Calcium Carbonate/Calcium Sulfonate Reverse Micelle, *J. Phys. Chem.* 100 (1996) 6637–6648, <https://doi.org/10.1021/jp951260j>.
- [33] B. Liu, M.I. Hoopes, M. Karttunen, Molecular dynamics simulations of DPPC/CTAB monolayers at the air/water interface, *J. Phys. Chem. B* 118 (2014) 11723–11737, <https://doi.org/10.1021/jp5050892>.
- [34] B. Fuglestad, K. Gupta, A.J. Wand, K.A. Sharp, Characterization of Cetyltrimethylammonium Bromide/Hexanol Reverse Micelles by Experimentally Benchmarked Molecular Dynamics Simulations, *Langmuir* 32 (2016) 1674–1684, <https://doi.org/10.1021/acs.langmuir.5b03981>.
- [35] E.M. Knipping, M.J. Lakin, K.L. Foster, P. Jungwirth, D.J. Tobias, R.B. Gerber, D. Dabdub, B.J. Finlayson-Pitts, Experiments and Simulations of Ion-Enhanced Interfacial Chemistry on Aqueous NaCl Aerosols, *Science* 288 (2000) (1979) 301–306, <https://doi.org/10.1126/science.288.5464.301>.
- [36] J.L. Thomas, M. Roeselova, L.X. Dang, D.J. Tobias, Molecular dynamics simulations of the solution-air interface of aqueous sodium nitrate, *Chem. A Eur. J.* 111 (2007) 3091–3098, <https://doi.org/10.1021/jp0683972>.
- [37] M.R. Harpham, B.M. Ladanyi, N.E. Levinger, K.W. Herwig, Water motion in reverse micelles studied by quasielastic neutron scattering and molecular dynamics simulations, *J. Chem. Phys.* 121 (2004) 7855–7868, <https://doi.org/10.1063/1.1792592>.
- [38] S. Abel, F. Sterpone, S. Bandyopadhyay, M. Marchi, Molecular Modeling and Simulations of AOT–Water Reverse Micelles in Isooctane: Structural and Dynamic Properties, *J. Phys. Chem. B* 108 (2004) 19458–19466, <https://doi.org/10.1021/jp047138e>.
- [39] M.R. Harpham, B.M. Ladanyi, N.E. Levinger, The effect of the counterion on water mobility in reverse micelles studied by molecular dynamics simulations, *J. Phys. Chem. B* 109 (2005) 16891–16900, <https://doi.org/10.1021/jp0527731>.
- [40] L. Kličová, E. Muchová, P. Šebej, P. Slavíček, P. Klán, Nature of CTAB/Water/Chloroform Reverse Micelles at Above- and Subzero Temperatures Studied by NMR and Molecular Dynamics Simulations, *Langmuir* 31 (2015) 8284–8293, <https://doi.org/10.1021/acs.langmuir.5b01776>.
- [41] J.A. da Silva, R.P. Dias, G.C.A. da Hora, T.A. Soares, M.R. Meneghetti, Molecular dynamics simulations of cetyltrimethylammonium bromide (CTAB) micelles and their interactions with a gold surface in aqueous solution, *J. Braz Chem Soc.* 29 (2018) 191–199. 10.21577/0103-5053.20170130.
- [42] J. Chowdhary, B.M. Ladanyi, Molecular Dynamics Simulation of Aerosol-OT Reverse Micelles, *J. Phys. Chem. B* 113 (2009) 15029–15039, <https://doi.org/10.1021/jp906915q>.
- [43] P. Mark, L. Nilsson, Structure and dynamics of the TIP3P, SPC, and SPC/E water models at 298 K, *Chem. A Eur. J.* 105 (2001) 9954–9960, <https://doi.org/10.1021/jp003020w>.
- [44] H.J.C. Berendsen, D. van der Spoel, R. van Drunen, GROMACS: A message-passing parallel molecular dynamics implementation, *Comput. Phys. Commun.* 91 (1995) 43–56, [https://doi.org/10.1016/0010-4655\(95\)00042-E](https://doi.org/10.1016/0010-4655(95)00042-E).
- [45] S. Páll, M. Abraham, C. Kutzner, B. Hess, E. Lindahl, Tackling Exascale Software Challenges in Molecular Dynamics Simulations with GROMACS, in: S. Markidis, E. Laure (Eds.), *Solving Software Challenges for Exascale*, Springer International Publishing, 2015; pp. 3–27. 10.1007/978-3-319-15976-8_1.
- [46] M.J. Abraham, T. Murtola, R. Schulz, S. Páll, J.C. Smith, B. Hess, E. Lindahl, GROMACS: High performance molecular simulations through multi-level parallelism from laptops to supercomputers, *SoftwareX*. 1–2 (2015) 19–25, <https://doi.org/10.1016/j.softx.2015.06.001>.
- [47] C. Kutzner, S. Páll, M. Fechner, A. Esztermann, B.L. de Groot, H. Grubmüller, Best bang for your buck: GPU nodes for GROMACS biomolecular simulations, *J. Comput. Chem.* 36 (2015) 1990–2008, <https://doi.org/10.1002/jcc.24030>.
- [48] B. Hess, C. Kutzner, D. van der Spoel, E. Lindahl, GROMACS 4: Algorithms for Highly Efficient, Load-Balanced, and Scalable Molecular Simulation, *J. Chem. Theory Comput.* 4 (2008) 435–447, <https://doi.org/10.1021/ct700301q>.
- [49] S. Pronk, S. Páll, R. Schulz, P. Larsson, P. Bjelkmar, R. Apostolov, M.R. Shirts, J.C. Smith, P.M. Kasson, D. van der Spoel, B. Hess, E. Lindahl, GROMACS 4.5: A high-throughput and highly parallel open source molecular simulation toolkit, *Bioinformatics*. 29 (2013) 845–854. 10.1093/bioinformatics/btt055.
- [50] J. Lee, X. Cheng, J.M. Swails, M.S. Yeom, P.K. Eastman, J.A. Lemkul, S. Wei, J. Buckner, J.C. Jeong, Y. Qi, S. Jo, V.S. Pande, D.A. Case, C.L. Brooks, A.D. Mackerell, J.B. Klauda, W. Im, CHARMM-GUI Input Generator for NAMD, GROMACS, AMBER, OpenMM, and CHARMM/OpenMM Simulations Using the CHARMM36 Additive Force Field, *J. Chem. Theory Comput.* 12 (2016) 405–413, <https://doi.org/10.1021/acs.jctc.5b00935>.
- [51] K. Vanommeslaeghe, E. Hatcher, C. Acharya, S. Kundu, S. Zhong, J. Shim, E. Darian, O. Guvench, P. Lopes, I. Vorobyov, A.D. Mackerell, CHARMM general force field: A force field for drug-like molecules compatible with the CHARMM all-atom additive biological force fields, *J. Comput. Chem.* 31 (2009) NA-NA, <https://doi.org/10.1002/jcc.21367>.
- [52] J.B. Klauda, R.M. Venable, J.A. Freites, J.W. O'Connor, D.J. Tobias, C. Mondragon-Ramirez, I. Vorobyov, A.D. Mackerell Jr., R.W. Pastor, J.W.O. Connor, D.J. Tobias, C. Mondragon-Ramirez, I. Vorobyov, A.D. Mackerell, R.W. Pastor, Update of the CHARMM all-atom additive force field for lipids, *J. Phys. Chem. B* 114 (2011) 7830–7843, <https://doi.org/10.1021/jp101759q>.
- [53] P. Bjelkmar, P. Larsson, M.A. Cuendet, B. Hess, E. Lindahl, Implementation of the CHARMM force field in GROMACS: Analysis of protein stability effects from correction maps, virtual interaction sites, and water models, *J. Chem. Theory Comput.* 6 (2010) 459–466, <https://doi.org/10.1021/ct900549r>.
- [54] L. Martínez, R. Andrade, E.G. Birgin, J.M. Martínez, L. Martínez, R. Andrade, E.G. Birgin, J.M. Martínez, PACKMOL: A package for building initial configurations for molecular dynamics simulations, *J. Comput. Chem.* 30 (2009) 2157–2164, <https://doi.org/10.1002/jcc.21224>.
- [55] U. Essmann, L. Perera, M.L. Berkowitz, T. Darden, H. Lee, L.G. Pedersen, A smooth particle mesh Ewald method, *J. Chem. Phys.* 103 (1995) 8577–8593, <https://doi.org/10.1063/1.470117>.
- [56] S. Strandé, H. Cai, M. Tatineni, W. Pfeiffer, C. Irving, A. Majumdar, D. Mishin, R. S. Sinkovits, M.M. Norman, N. Wolter, T. Cooper, I. Altintas, M. Kandes, I. Perez, M. Shantharam, M. Thomas, S. Sivagnanam, T. Hutton, H. Cai, T. Cooper, C. Irving, T. Hutton, M. Kandes, A. Majumdar, D. Mishin, I. Perez, W. Pfeiffer, M. Shantharam, R.S. Sinkovits, S. Sivagnanam, S. Strandé, M. Tatineni, M. Thomas, N. Wolter, M.M. Norman, T. Hut-ton, Expanse: Computing without Boundaries: Architecture, Deployment, and Early Operations Experiences of a Supercomputer Designed for the Rapid Evolution in Science and Engineering, in: *Practice and Experience in Advanced Research Computing*, Association for Computing Machinery, New York, NY, USA, 2021. 10.1145/3437359.
- [57] J. Towns, T. Cockerill, M. Dahan, I. Foster, K. Gaither, A. Grimshaw, V. Hazlewood, S. Lathrop, D. Lifka, G.D. Peterson, R. Roskies, J.R. Scott, N. Wilkins-Diehr, XSEDE: Accelerating Scientific Discovery, *Comput. Sci. Eng.* 16 (2014) 62–74, <https://doi.org/10.1109/MCSE.2014.80>.
- [58] A.V. Martinez, L. Dominguez, E. Malolepsza, A. Moser, Z. Ziegler, J.E. Straub, Probing the Structure and Dynamics of Confined Water in AOT Reverse Micelles, *J. Phys. Chem. B* 117 (2013) 7345–7351, <https://doi.org/10.1021/jp402270e>.
- [59] R. Sett, S. Sen, B.K. Paul, N. Guchhait, How Does Nanoconfinement within a Reverse Micelle Influence the Interaction of Phenazinium-Based Photosensitizers with DNA?, *ACS Omega* 3 (2018) 1374–1385, <https://doi.org/10.1021/acsomega.7b01820>.
- [60] B.K. Paul, D. Ray, N. Guchhait, Binding interaction and rotational-relaxation dynamics of a cancer cell photosensitizer with various micellar assemblies, *J. Phys. Chem. B* 116 (2012) 9704–9717, <https://doi.org/10.1021/jp304280m>.
- [61] Hydrogen bonds – GROMACS 2022.4 documentation, (n.d.), <https://manual.gromacs.org/current/reference-manual/analysis/hydrogen-bonds.html> (accessed November 29, 2022).
- [62] D. Laage, W.H. Thompson, Reorientation dynamics of nanoconfined water Power-law decay, hydrogen-bond jumps, and test of a two-state model, *J. Chem. Phys.* 136 (2012) 1–7, <https://doi.org/10.1063/1.3679404>.
- [63] G. Eskici, P.H. Axelsen, The Size of AOT Reverse Micelles, *J. Phys. Chem. B* 120 (2016) 11337–11347, <https://doi.org/10.1021/acs.jpcc.6b06420>.